Human-machine Collaboration Modalities for Semi-automated Needle Insertion Into Soft Tissue

Thomas Lehmann[1], Ronald Sloboda[2], Nawaid Usmani[3], and Mahdi Tavakoli[1]

***Abstract*—Needle insertion is a minimally invasive medical procedure commonly used for biopsy, ablation or deposition of therapeutic agents. In prostate brachytherapy, needles are inserted into the prostate in order to deposit multiple rice-grain-sized radioactive seeds to eradicate cancerous tissue from close proximity. During insertion, the needles should remain on a straight path, such that the seeds are deposited according to their pre-planned location. The needles, however, due to their beveled tip, deflect from the straight path. In order to guide the needle back towards the straight path, the surgeon may manually rotate the needle axially or apply lateral force onto the needle near its entry point into tissue. To aid the surgeon with steering the needle more accurately towards the desired target, we propose robotic assistance where the responsibilities are assigned between the surgeon and the machine in such a way that safety is guaranteed while achieving high steering accuracy. Thus, in this work, a human-in-the-loop collaborative robotic assistant system is proposed where the aforementioned steering actions are carried out autonomously by the robotic assistant system. This collaboration modality is in agreement with safety requirements as the surgeon remains in the loop and is in charge of the most safety-critical task, which is the needle insertion itself. It is shown experimentally that using both steering commands from the machine as the surgeon inserts the needle satisfactorily achieves the goal of minimizing needle deflection with high accuracy.**

***Index Terms*—Medical Robots and Systems; Surgical Robotics: Steerable Catheters/Needles**

I. Introduction

NEEDLE insertion is a minimally invasive medical procedure in which subcutaneous needles are inserted into various regions of the body for the purpose of ablation, biopsy, drug delivery or cancer therapy. Prostate brachytherapy is a therapeutic procedure in which rice-grain sized radioactive seeds are permanently implanted within the prostate in order to eradicate cancerous tissue. A schematic representation of the procedure is illustrated in Fig. 1. Brachytherapy needles that house the radioactive seeds are inserted into the prostate followed by deposition of the seeds within and around cancerous tissue. The seeds then apply a defined dosage of radiation to the cancerous tissue from close proximity, thus more directly affecting the cancer while reducing radiation exposure to surrounding healthy tissue and organs. Brachytherapy is a promising alternative to other cancer treatment procedures such as beam radiation therapy as it is more patient friendly and less time consuming and carries high success rates in terms of tumour reduction.

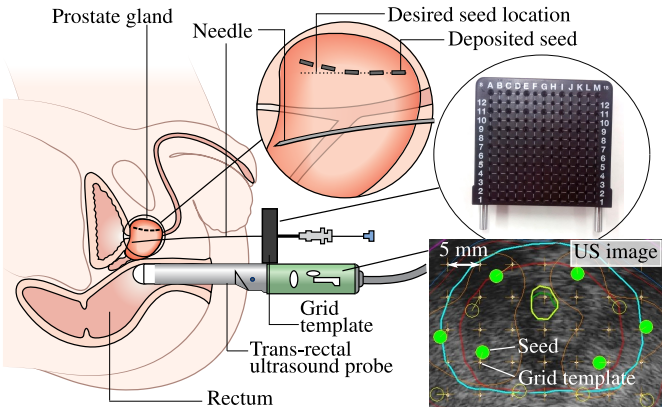

Fig. 1. A schematic representation of the radiation therapy procedure prostate brachytherapy. Radioactive seeds are implanted within the prostate with a needle guided by a grid template. The location of seed deposition is observed with a trans-rectal ultrasound (TRUS) probe (source: Cancer Research UK / Wikimedia Commons).

During the pre-planning phase of each procedure, seed locations are chosen to ensure effective distribution of radiation dosage. The locations of seed deposition within the prostate are chosen based on a discrete 5 mm spacing defined by the grid template (see Fig. 1) so that seeds are placed on the grid template markings (see Fig. 1, US image). This is to facilitate a distribution of radiation according to the pre-planned distribution. A critical assumption during pre-planning is that the needle remains on a straight path during insertion. In clinical practice, however, this assumption does not hold well as the needle deflects from the desired straight path during insertion due to its beveled tip. Needle deflection can cause the seeds to be misplaced from their desired location within the prostate, which in turn causes inefficient distribution of radiation. To correct for needle deflection and bring the needle

Manuscript received: May 23, 2017; Revised September 6, 2017; Accepted October 9, 2017.

This paper was recommended for publication by Editor Allison M. Okamura upon evaluation of the Associate Editor and Reviewers' comments. This work is supported by the Canada Foundation for Innovation (CFI) under grant LOF 28241, the Alberta Innovation and Advanced Education Ministry under Small Equipment Grant RCP-12-021, the Natural Sciences and Engineering Research Council (NSERC) of Canada under grant CHRP 446520, the Canadian Institutes of Health Research (CIHR) under grant CPG 127768, the Alberta Innovates - Health Solutions (AIHS) under grant CRIO 201201232 and by a University of Alberta startup grant.

[1]Thomas Lehmann (Corresponding Author) and Mahdi Tavakoli are with the Department of Electrical and Computer Engineering, University of Alberta, AB, Canada T6G 1H9. {lehmann, mahdi.tavakoli}@ualberta.ca

[2]Ronald Sloboda is with the Division of Medical Physics, Department of Oncology, Cross Cancer Institute, 11560 University Avenue, Edmonton, AB, Canada T6G 1Z2. ron.sloboda@albertahealthservices.ca.

[3]Nawaid Usmani is with the Department of Oncology, Cross Cancer Institute, 11560 University Avenue, Edmonton, AB, Canada, T6G 1Z2. nawaid.usmani@albertahealthservices.ca

Digital Object Identifier (DOI): see top of this page.

back to a straight path, the surgeon may intermittently axially rotate the needle by 180° at an ideal insertion depth (rotation depth). This causes the direction of the forces acting at the beveled needle tip that are responsible for needle deflection to be inverted and thus steers the needle back to the desired straight path. The needle deflection needs to be controlled by an experienced surgeon such that the deflected needle shape at the final insertion depth is as close to the unbent needle as possible (see Fig. 1) through the choice of an appropriate insertion depth at which the intermittent axial rotation is carried out (rotation depth).

A further needle steering input used manually by surgeons is the application of lateral force onto the needle. The force is applied near the needle's entry point in tissue against the direction of deflection using the finger early on during insertion. The lateral force enacted by the finger results in lateral needle displacement against the direction of deflection caused by the beveled needle tip.

To enhance needle steering, the utilization of robotic assistance for needle insertion has been the subject of substantial research for over a decade. Investigated topics towards the development of robotic needle steering are needle-tissue interaction modeling, needle deflection modeling and estimation, automatic needle steering and deflection control algorithms, needle deflection feedback using medical imaging modalities (e.g., ultrasound), and robotic systems design. A comprehensive literature review on current issues in closed-loop needle steering is provided by Rossa and Tavakoli [1].

The developed needle steering concepts and robotic systems for needle steering can be divided into three automation levels (see Fig. 2): *Level 3*: fully automated steering [2]–[7]; *Level 2*: semi-automated steering (surgeon-in-the-loop) [8]–[13]; *Level 1*: assisted manual steering (enhancing the surgeon's awareness through haptics cues, etc.) [14]–[19]. The current clinical practice involves no automation of the needle steering task (fully manual needle steering). Each of these automation levels have various advantages and disadvantages, which will be further elaborated on in Section II.

While in the past intermittent or continuous axial needle rotation has been the primary steering action [20]–[23], the second above-mentioned steering action being the lateral application of force somewhere on the needle (near the needle entry point into tissue) has not been considered extensively for robotic needle steering. In this work, a collaborative approach between human and machine is introduced that provides robotic assistance for steering actions while also presenting an initial analysis on the effect of lateral actuation on reducing needle deflection. A combination of the two steering actions intermittent axial rotation and lateral actuation that are currently carried out manually during brachytherapy are performed automatically by a robotic assistance system while the needle is inserted fully manually by the surgeon such that the surgeon is in charge of the most safety-critical tasks during the needle insertion procedure. Thus, this system represents a human-in-the-loop collaborative robotic assistant system. With this assignment of responsibilities, the steering accuracy of fully automated insertion is retained while the procedure's safety remains guaranteed by keeping the surgeon

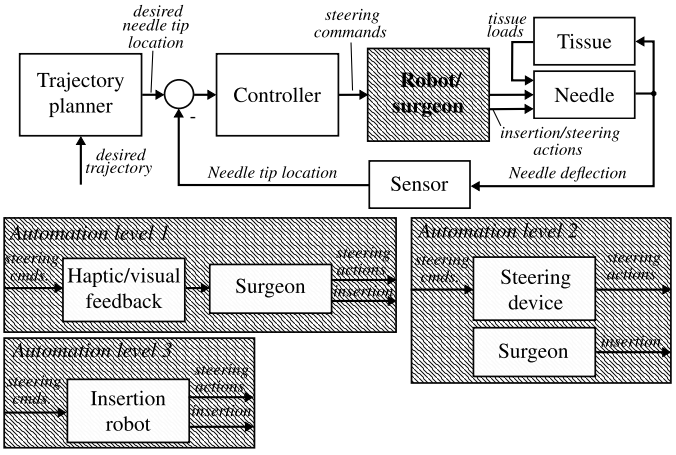

Fig. 2. The three automation levels for robotics-assisted needle steering.

in the loop. Moreover, we present the advantages of using steering inputs (axial rotation and lateral actuation) simultaneously for minimizing both the needle tip deflection and achieving an unbent needle shaft at the final insertion depth. Particularly the requirement of an unbent needle at the final insertion depth is important during prostate brachytherapy to ensure seed placement along a straight line. When, however, the number of rotations needs to be limited in order to avoid tissue trauma, this objective is difficult to achieve.

II. Human-machine Collaboration Modalities

Fig. 2 shows the concept of needle steering as a block diagram. A needle steering system consists of the needle-tissue system where the needle deflects as it is inserted into tissue. The needle tip location can be tracked using medical imaging modalities for feedback control of the needle deflection. A trajectory planner determines the desired needle tip location based on a desired trajectory and a controller minimizes the error between desired and measured needle tip location through supplying appropriate steering commands to either the robotic system or surgeon, depending on the automation level.

The allocation of actions to either a machine or the surgeon is classified into three categories, namely automation levels 3, 2 and 1. For a system of the type automation level 3, an autonomous robotic system is in complete control of the insertion and carrying out the steering actions commanded by the controller. In this automation level, human involvement is entirely eliminated from the needle insertion procedure. A major challenge with automation level 3 is, however, to guarantee the stability and safety of the robotic system, which is difficult in an uncertain environment such as the human body. This causes issues with clinical acceptance, which makes clinical implementation of systems with automation level 3 difficult.

To help mitigate these issues, automation levels 1 or 2 can be considered where the surgeon remains in charge of safety-critical tasks such as the insertion itself or steering actions, depending on the automation level. Considering a system of automation level 2, the controller provides steering

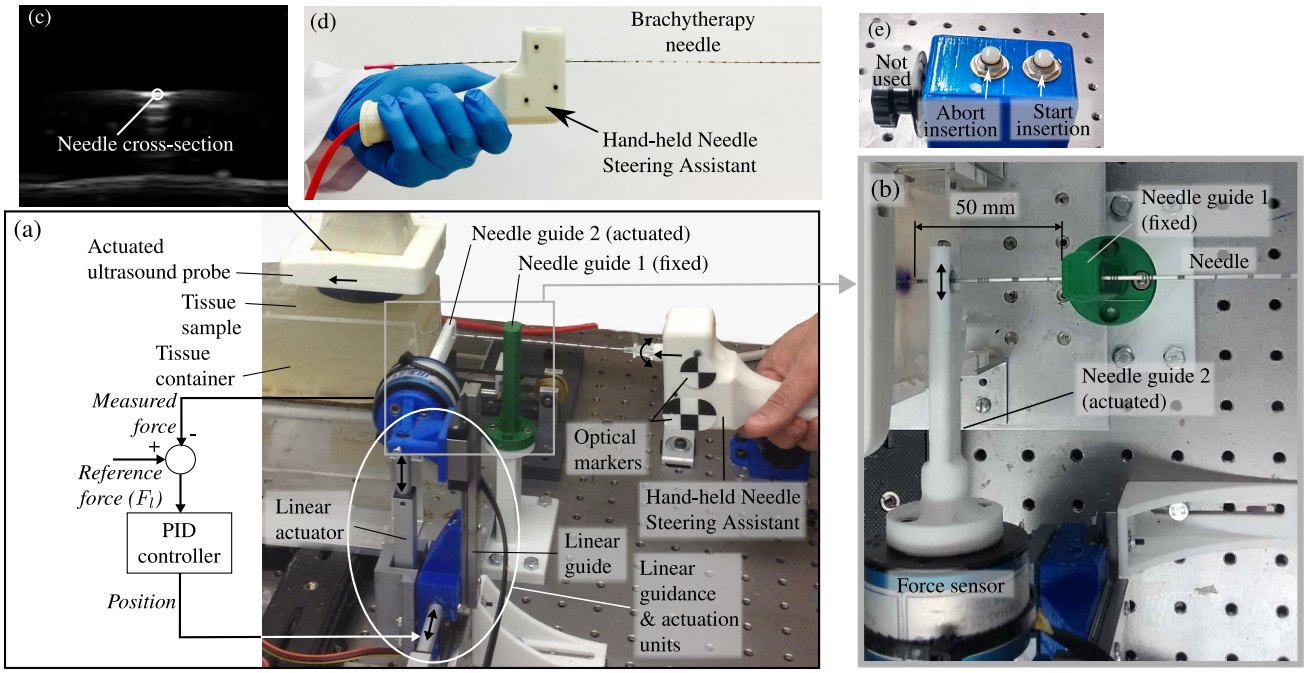

Fig. 3. The robotic needle insertion prototype system with (a) the total perspective of the setup, (b) a top-down close-up view of the needle being guided through the actuated and fixed needle guides, (c) an ultrasound image taken by the actuated ultrasound transducer showing the needle cross-section as a bright spot, (d) a close-up image of the Hand-held Needle Steering Assistant, and (e) a control panel for the user to indicate the start or abortion of an insertion.

commands to a device that automatically carries out commanded steering actions while the surgeon remains in charge of needle insertion. This scenario is commonly referred to as surgeon-in-the-loop. Finally, automation level 1 represents the least automated level where only visual or haptic information, guidance and suggestions are provided to the surgeon based on the controller output. The final decision as to whether the action is carried out remains solely with the surgeon, which makes automation level 1 the safest. When considering the example of needle insertion, however, executing both steering actions simultaneously and manually while also inserting the needle, as would be the case in automation level 1 can be overwhelming for the human, which leads to mistakes and inaccurate needle steering. Therefore in this work, the robotic assistant system controls the steering actions while the surgeon remains in charge of needle insertion in accordance with automation level 2. The hypothesis is that the lateral force can help with this goal while the amount of necessary needle rotations can be limited to only one in order to minimize tissue trauma.

To show that using both steering inputs simultaneously helps reduce the needle deflection shape at the final insertion depth, insertion experiments are carried out where a constant lateral force is applied during a section of the insertion. During the same insertion, one rotation is carried out at a depth that minimizes the needle tip deflection at the final insertion depth. Two more scenarios are considered where only one of the steering inputs is used in each scenario. The three scenarios and parameter settings of the steering inputs are listed in Table I.

III. Robotic Assistant System Prototype

The experimental robotic assistant system prototype used to carry out needle insertions is depicted in Fig. 3. The system was designed to replicate a typical clinical scenario as found during prostate brachytherapy with added needle and ultrasound transducer actuation systems that seamlessly integrate into a clinical setup. The setup consists of the Hand-held Needle Steering Assistant (HNSA, see Fig. 3d) [10], the linear guidance and actuation unit, and an actuated ultrasound (US) transducer. A needle (e.g., a standard brachytherapy needle) is rigidly connected to the HNSA such that it can be inserted manually into tissue using the HNSA. An optical motion tracker (MicronTracker 3, ClaroNav, Toronto, ON, Canada, not included in Fig. 3) measures the current horizontal location of the HNSA via optical markers. The tracker's RMS error is 0.32 mm. Since the motion tracker is calibrated to the tissue container and the needle is assumed a rigid body in insertion direction, the current needle insertion depth can be inferred from the measured HNSA location. The HNSA contains a miniature DC motor through which the needle can be rotated axially at a desired insertion depth. Further details on the HNSA are given in [10].

During insertion, the needle is guided by needle guide 1 (fixed) and needle guide 2 (actuated). While guide 1, which resembles the grid template used during brachytherapy, prevents the needle from pivoting, guide 2 is designed to allow the needle to pivot. Needle guide 2 can be displaced laterally to the axial needle direction through two perpendicularly mounted linear guidance and actuation units. Each linear guidance and actuation unit consists of a Miniature Linear Guide (Type SSEBV16-150, MISUMI Group Inc., Tokyo, Japan) and a L16

Miniature Linear Actuator (Actuonix Motion Devices Inc., Victoria, BC, Canada). The units are mounted in serial and confine needle guide 2's motions to a plane normal to the axial needle direction. In this work, only the horizontal actuator is used to apply force onto the needle while the vertical actuator is used to vertically align needle guide 2 with needle guide 1.

A JR3 force sensor (Type 50M31A3-I25, JR3 Inc., Woodland, CA, USA) mounted between needle guide 2 and the linear actuation units measures the horizontal and vertical forces enacted onto the needle by displacement of guide 2. The force-position-based control scheme (see Fig. 3a) was chosen because the linear actuator's hardware controller only accepts positions as input. Thus, to control the amount of lateral force supplied to the needle by needle guide 2, the PID controller adjusts the actuated needle guide's position to match the desired force.

The needle tip trajectory during insertion (e.g., the path cut by the needle tip during insertion) and needle deflection are measured using transversal US images acquired by a clinical US system. The US system consists of a transducer (Model 4DL14-5/38 Linear 4D, Ultrasonix, Richmond, BC, Canada) and a diagnostic US system (Model SonixTOUCH, Ultrasonix, Richmond, BC, Canada), which generates US images from sonography data acquired by the transducer. The US transducer is actuated and can be controlled to continuously track the needle tip within tissue during insertion. A sample transverse image of the needle cross-section within phantom tissue is shown in Fig. 3c where the needle cross-section appears as a bright spot. The location of the needle cross-section within acquired US images and therefore the needle deflection is tracked in real-time with an enhanced version of the algorithm proposed in [24]. The pixel quantization accuracy for US images is 0.05 millimeters per pixel.

IV. Simulation of Lateral Actuation

A simple needle deflection model based on Euler-Bernoulli beam theory is introduced in this section for the simulation of the needle's deflection when a lateral point load is applied. Of particular interest is how the insertion depth impacts the needle deflection, especially the deflection slope at the needle tip. From this information, conclusions on the insertion depth at which the lateral force should be applied in order to achieve the maximum reduction in needle deflection at the final insertion depth can be drawn. Fig. 4a shows the modeled forces and moments acting on the needle as it is displaced by the lateral point load F_l. q_t is the reaction load enacted by tissue onto the needle caused by the displacement. For the sake of simplicity, q_t is assumed to be uniform. F_R and M_R are the reaction force and moment, respectively, enacted by the fixed needle guide that is modeled as a clamping.

The clamped needle-tissue system shown in Fig. 4a can be expressed as

$$EI\frac{d^4u(z)}{dz^4} = F_l\langle z-c_2\rangle^{-1} - q_t\langle z-c\rangle^0 \tag{1}$$

where $u(z)$ is the needle deflection, c_2 is the distance between the fixed to the actuated needle guide and $c = c_1 + c_2$ is the distance between the fixed needle guide and the tissue. The loads F_l and q_t in (1) are modeled by the following discontinuous function [25]

$$\langle z-c\rangle^n = \begin{cases} 0 & \text{when } z \le c \\ (z-c)^n & \text{when } z > c \end{cases} \quad \text{if } n = 0,1,2,...$$
$$\langle z-c\rangle^n = \begin{cases} +\infty & \text{when } z = c \\ 0 & \text{when } z \neq c \end{cases} \quad \text{if } n = -1.$$

To solve for the needle deflection $u(z)$, (1) needs to be integrated four times. The first integration of (1) yields the shear force $V(z)$

$$V(z) = F_l\left(1 - \langle z-c_2\rangle^0\right) + q_t\left((l-c) - \langle z-c\rangle^1\right) \tag{2}$$

when using the known boundary condition at the needle tip $V(l) = 0$ to solve for the constant of integration. Integrating (2) yields the bending moment $M(z)$

$$\begin{aligned} M(z) &= F_l\left[(z-c_2) - \langle z-c_2\rangle^1\right] \\ &\quad + q_t\left[(l-c)z - \frac{\langle z-c\rangle^2}{2} + \frac{c^2-l^2}{2}\right] \end{aligned} \tag{3}$$

when using the known boundary condition at the needle tip $M(l) = 0$ to solve for the constant of integration. Integrating (3) twice more yields the needle deflection $u(z)$

$$\begin{aligned} u(z) &= \frac{1}{24EI}\left[F_l\left(4z^3 - 4\langle z-c_2\rangle^3 - \frac{c_2}{2}z^2\right)\right. \\ &\quad \left. - q_t\left(\langle z-c\rangle^4 - 6(l-c)z^3 - 6\left(c^2-l^2\right)z^2\right)\right] \end{aligned} \tag{4}$$

when using the known boundary conditions at $z = 0$ where $u'(0) = 0$ and $u(0) = 0$ to solve for the constants of integration.

The next step is to find a linear system of three equations to solve for the unknowns F_R, M_R and q_t. For the first equation, (2) can be used in combination with the boundary condition $V(0) = F_R$:

$$V(0) = F_R = -q_t(l-c) - F_l \rightarrow F_l = -F_R - q_t(l-c) \tag{5}$$

and for the second equation, (3) can be used in combination with the boundary condition $M(0) = -M_R$:

$$M(0) = -M_R = -F_l c_2 + \frac{q_t\left(c^2-l^2\right)}{2} \rightarrow F_l = \frac{M_R}{c_2} - \frac{q_t\left(c^2-l^2\right)}{2} \tag{6}$$

A third equation can be established as follows:

$$\begin{aligned} M(c) &= -F_R c - M_R + q_t\frac{d^2}{2} + F_l c_1 = 0 \\ \rightarrow F_l &= \frac{F_R c}{c_1} + \frac{M_R}{c_1} - q_t\frac{d^2}{2c_1} \end{aligned} \tag{7}$$

when considering that equilibrium must be maintained. The linear system of equations is then

$$\begin{bmatrix} -1 & 0 & -(l-c) \\ 0 & \frac{1}{c_2} & -\frac{c^2-l^2}{2} \\ \frac{c}{c_1} & \frac{1}{c_1} & -\frac{d^2}{2c_1} \end{bmatrix} \begin{bmatrix} F_R \\ M_R \\ q_t \end{bmatrix} = F_l \mathbf{1}_{3\times 1} \tag{8}$$

Simulation results for the three insertion depths 10, 20 and 30 mm are plotted in Fig. 4b. The plots show that the orientation of the needle tip and therefore its heading can be directly

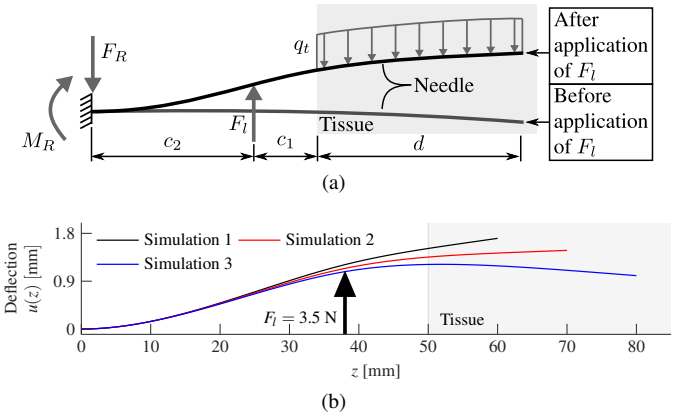

Fig. 4. (a) a schematic representation of the clamped needle inserted into tissue with a lateral point load F_l applied at $z = c_1$ and the reactions due to needle clamping (F_R and M_R), and tissue displacement q_t. (b) Simulation results considering the three simulated needle insertion depths 10, 20 and 30 mm.

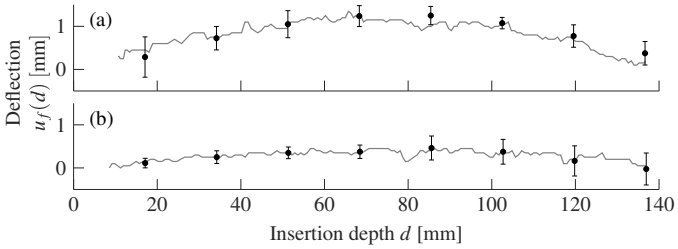

Fig. 5. The needle deflection at the final insertion depth $u_f(d)$ for one insertion during (a) scenario 1 and (b) scenario 3 after the needle is inserted into *phantom* tissue. Average deflection including error bars are plotted in both (a) and (b).

manipulated by using lateral force where the insertion depth at which the force is applied influences the amount of achievable tip orientation change. For each insertion depth, the needle tip heading and deflection differ whereas at shallower depth (e.g., Simulation 1), the change in needle tip heading is much higher. Supposing that the needle is further inserted beyond the depths shown in Fig. 4b while the lateral force F_l is still applied, the most reduction of needle deflection could presumably be achieved with force application according to Simulation 1. This simulated behavior of the needle makes physical sense due to a combination of the needle's decreased resistance to bending and a greater amount of the needle being embedded in tissue with increased length. Moreover, the needle shapes plotted in Fig. 4 show a similar needle tip deflection than the experimental measurements of the needle tip deflection plotted in Fig. 7b and Fig. 8b at equivalent insertion depths. This indicates that the deflection model represents the behavior of the needle when applying the lateral force F_l with sufficient accuracy. The conclusion from this simulation is thus that lateral force needs to be applied early to maximize its effect with respect to reduction of deflection.

V. Experimental Study

A. Protocol

To evaluate the ability to minimize needle deflection for various combinations of the two needle steering inputs lateral actuation and axial rotation, three scenarios are considered. The scenarios are listed in Table I where in the first two scenarios, only one of the steering inputs is considered while in scenario 3, both inputs are used simultaneously. In each scenario, a standard 18 gauge brachytherapy needle (Type RP-1100-1820, Riverpoint Medical, Portland, OR, USA) is inserted manually into a phantom tissue sample made from Plastisol (Type Super Soft Plastic, M-F Manufacturing Co., Inc, Fort Worth, TX, USA) and an ex-vivo porcine loin tissue sample using the Hand-held Needle Steering Assistant described in Section III and [10]. The final insertion depth d_f is 140 mm. The stiffness of the phantom tissue sample was adjusted to 11 kPa using a ratio of 1/4 plastic softener to Plastisol.

TABLE I
THE THREE CONSIDERED EXPERIMENTAL SCENARIOS. ROTATION AND LATERAL ACTUATION ARE DONE BY MACHINE, INSERTION MANUALLY.

Scenario	Rotation	Lateral actuation	Rotation depth [mm]	Applied force(s) [N]
1	yes	no	35	n/a
2	no	yes	n/a	-[2, 2.5, 3, 3.5]
3	yes	yes	50	-3.5

The optimal values of the steering action parameters rotation depth d_r, and lateral force profile F_l were determined empirically during preliminary experiments informed by the simulation results presented in Section IV and by the advice of an oncologist carrying out prostate brachytherapy procedures. The choice of the steering action parameters is so that the needle tip deflection at the final insertion depth and also the deflection of the entire needle are at a minimum as it is desired in prostate brachytherapy. The rotation depth d_r for scenario 1 and 3 were chosen so that the needle tip deflection at the final insertion depth is minimized. The lateral force quantity F_l was chosen for the same purpose but also to minimize the deflection of the entire needle at the final insertion depth. Four runs were carried out under scenario 1 and 3. Regarding scenario 2, it was found during the preliminary experiments that the achievable reduction of needle deflection when using only lateral force is rather limited. For this reason, no single optimal lateral force could be found and the results of the preliminary experiments (see Table I, row 2) are presented in the following.

In all scenarios where lateral actuation is used, the constant force indicated in Table I is applied for an insertion depth range of 20 to 100 mm (see also Fig. 7a and Fig. 8a). This range was empirically determined based on a maximization of the lateral force's effect so that the force is removed when its influence on needle tip deflection is no longer apparent. To record the needle deflection after stopping insertion at the final depth, the actuated US transducer was moved from the needle tip towards the needle entry point into tissue at a velocity of 15 mm/s.

The only interactions between human and machine are to signal the start of an insertion with the press of a button (see

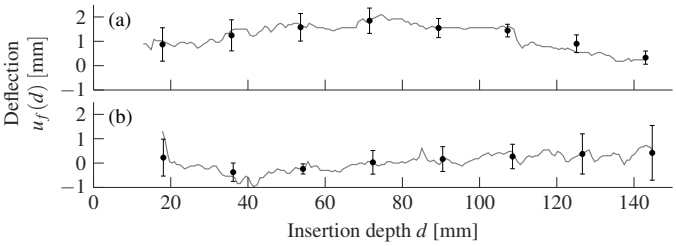

Fig. 6. The needle deflection at the final insertion depth $u_f(d)$ for one insertion during (a) scenario 1 and (b) scenario 3 after the needle is inserted into *porcine* tissue. Average deflection including error bars are plotted in both (a) and (b).

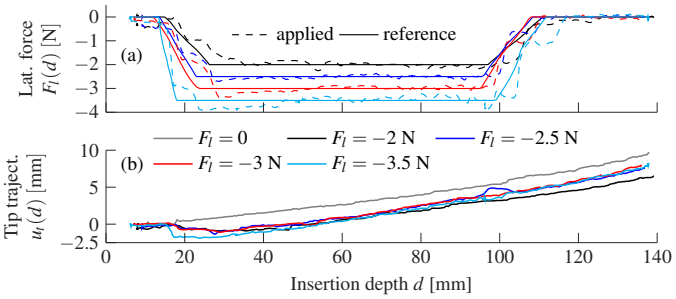

Fig. 7. Needle insertion during scenario 2 into *phantom* tissue: (a) various applied lateral force profiles and (b) the corresponding needle tip trajectories (e.g., the paths cut by the needle tip) during insertion.

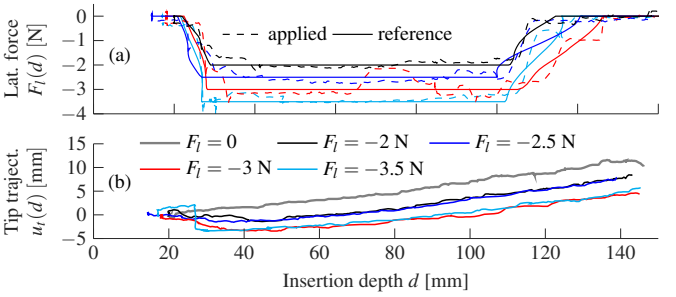

Fig. 8. Needle insertion during scenario 2 into *porcine* tissue: (a) various applied lateral force profiles and (b) the corresponding needle tip trajectories (e.g., the paths cut by the needle tip) during insertion.

Fig. 3e) and the display of the current insertion depth on a screen.

B. Results

In Fig. 5, the needle deflections at the final insertion depth for one run and during scenario 1 (Fig. 5a) and 3(Fig. 5b) are plotted along with averages among all four runs at various depths and error bars. When comparing the amount of deflection $u_f(d)$ shown in Fig. 5a and Fig. 5b, and Fig. 6a and Fig. 6b, less deflection can be observed during scenario 3 than during scenario 1 for both the phantom and porcine tissue.

Fig. 7 and Fig. 8 illustrate the results under scenario 2 for phantom and porcine tissue, respectively, according to Table I where Fig. 7a and Fig. 8a plot the applied forces, and Fig. 7b and Fig. 8b plot the corresponding needle tip trajectories. The needle tip deflection at the final insertion depth does not fall below approximately 7 mm regardless of the applied lateral force for the phantom tissue and not below 5 mm for the porcine tissue. For comparison, the needle tip trajectory for an insertion with no steering actions is also plotted in Fig. 7b and Fig. 8b. The 2 mm and 6 mm reductions in needle tip deflection at the final insertion depth are not by themselves substantial.

TABLE II
STATISTICAL RESULTS OF SCENARIOS 1 AND 3. $|A_e|$ IS THE ABSOLUTE AREA UNDER THE NEEDLE DEFLECTION SHAPE, $\max(u_f)$ IS THE MAXIMUM OF THE OBSERVED DEFLECTION OF THE NEEDLE DEFLECTION u_f, AND $u_t(d_f)$ IS THE NEEDLE TIP DEFLECTION AT THE FINAL INSERTION DEPTH d_f.

Scenario	Tissue		Average $\lvert A_e\rvert$ [mm^2]	Average $\max(u_f)$ [mm]	Average $u_t(d_f)$ [mm]
1	Phantom		112.87±29.33	1.39±0.23	0.4±0.3
	Porcine		165.37±50.57	2.07±0.32	0.28±0.34
3	Phantom		42.22±24.15	0.53±0.25	0±0.3
	Porcine		61.78±23.01	1.05±0.47	0.46±0.34
t-test	Phantom	h	unequal	unequal	equal
		p-value	0.01	0.002	0.09
	Porcine	h	unequal	unequal	equal
		p-value	0.01	0.01	0.77

In Table II, statistical results comparing the deflection shapes for scenarios 1 and 3 are listed. Scenario 2 was omitted in the analysis provided in Table II as the results depicted in Fig. 7 clearly show insufficient reduction of deflection and thus no need for additional analysis. The mean of the absolute area under the needle deflection shape $|A_e|$ is significantly lower for insertions carried out under scenario 3 compared to scenario 1 with a difference of approximately 70 mm^2 for phantom tissue and 104 mm^2 for porcine tissue. The same can be observed for the mean of the maximum needle deflection $\max(u_f)$ with a difference of approximately 0.9 mm for phantom tissue and 1 mm for porcine tissue. A two-sampled t-test evaluates whether a statistically significant difference between scenarios 1 and 3 for the average $|A_e|$ and the average $\max(u_f)$ exists. This shows whether significant improvement in needle deflection minimization was made under scenario 3 compared to scenario 1. The test decision given in Table II for both phantom and porcine tissue, indicates that for both cases the null hypothesis must be rejected at the 5% significance level so that the $|A_e|$ and the average $\max(u_f)$ are statistically significantly different. This implies that the means are unequal. The average needle tip deflection at the final insertion depth $u_f(140mm)$ for scenario 1 and 3 is given in the last column of Table II. Although differences of 0.4 mm for the phantom tissue and 0.18 mm for the porcine tissue exist, the t-test decision shows no statistically significant difference.

VI. DISCUSSION

The comparison between scenario 1 and 3 shows that using both steering inputs according to scenario 3 results in an almost entirely straight needle at the final insertion depth with very little remaining deflection. Both the maximum needle deflection and the absolute area under the needle (see Table II, $|A_e|$) are significantly smaller for scenario 3 compared to scenario 1. The results presented for scenario 3 show that the

needle deflection can be successfully minimized while both steering inputs axial rotation and lateral actuation are automated and insertion is carried out manually. This indicates a lower learning curve for novice surgeons, which helps to level out the seed placement accuracy curve for experienced and novice surgeons. When only lateral actuation is used as needle steering input (scenario 2), although the needle deflection is reduced, the ability to minimize needle deflection is limited (see Fig. 7 and Fig. 8) meaning that also the steering effect is limited. When combined with axial needle rotation as steering input, however, considerable improvements are obtained. It is shown that the lateral force plays a supplementary but vital role besides axial rotation as far as reducing the needle deflection is concerned. It should be noted that during the experiments in this paper, the distance between the fixed needle guide (guide 1) and the tissue sample was 50 mm (see Fig. 3). It is presumed that the impact of the lateral actuation steering input with respect to needle deflection might significantly improve with reduced distance between fixed guide to tissue.

It could be argued that lateral needle actuation can cause safety issues for the patient in case of instability of the force controller. This issue can be avoided by inhibiting the lateral force by mechanically limiting the maximum displacement such that the maximum force that may be applied by the actuator is also limited. Furthermore, the actuator can be chosen so that its maximum mechanical energy does not exceed the maximally allowed energy introduced into the body.

VII. Conclusion & Future Work

This work introduces a collaborative human-in-the-loop approach for needle steering in prostate brachytherapy. It is experimentally shown that using the steering input lateral needle actuation along with axial needle rotation can help to further minimize needle deflection. This illustrates the advantage of a robotics-actuated needle insertion device where the responsibilities are distributed among the surgeon and the machine to maximize the safety of the procedure while preserving high steering accuracy. Our future work will be concerned with further investigating lateral needle actuation as needle steering input by developing control algorithms that adjust the lateral force applied to the needle intelligently based on model-based prediction.

References

[1] C. Rossa and M. Tavakoli, "Issues in closed-loop needle steering," *Control Engineering Practice*, vol. 62, pp. 55–69, May 2017.

[2] H. Bassan, R. Patel, and M. Moallem, "A Novel Manipulator for Percutaneous Needle Insertion: Design and Experimentation," *IEEE/ASME Trans. Mechatron.*, vol. 14, no. 6, pp. 746–761, Dec. 2009.

[3] N. Hungr, M. Baumann, J.-A. Long, and J. Troccaz, "A 3-D Ultrasound Robotic Prostate Brachytherapy System With Prostate Motion Tracking," *IEEE Trans. Robot.*, vol. 28, no. 6, pp. 1382–1397, Dec. 2012.

[4] M. Muntener, A. Patriciu, D. Petrisor, D. Mazilu, H. Bagga, L. Kavoussi, K. Cleary, and D. Stoianovici, "Magnetic resonance imaging compatible robotic system for fully automated brachytherapy seed placement," *Urology*, vol. 68, no. 6, pp. 1313–1317, Dec. 2006.

[5] L. Phee, Di Xiao, J. Yuen, Chee Fatt Chan, H. Ho, Choon Hua Thng, Christopher Cheng, and Wan Sing Ng, "Ultrasound Guided Robotic System for Transperineal Biopsy of the Prostate," in *Proc. IEEE Int. Conf. Robotics and Automation (ICRA)*, April 2005, pp. 1315–1320.

[6] R. Webster, J. Memisevic, and A. Okamura, "Design Considerations for Robotic Needle Steering," in *Proc. IEEE Int. Conf. Robotics and Automation (ICRA)*, April 2005, pp. 3588 – 3594.

[7] Z. Wei, G. Wan, L. Gardi, D. B. Downey, and A. Fenster, "Robotic-aided 3D TRUS guided intraoperative prostate brachytherapy." International Society for Optics and Photonics, May 2004, p. 361.

[8] G. Fichtinger, J. P. Fiene, C. W. Kennedy, G. Kronreif, I. Iordachita, D. Y. Song, E. C. Burdette, and P. Kazanzides, "Robotic assistance for ultrasound-guided prostate brachytherapy," *Medical Image Analysis*, vol. 12, no. 5, pp. 535–545, June 2008.

[9] S. Okazawa, R. Ebrahimi, J. Chuang, S. E. Salcudean, and R. Rohling, "Hand-held steerable needle device," *IEEE/ASME Trans. on Mechatron.*, vol. 10, no. 3, pp. 285–296, June 2005.

[10] C. Rossa, N. Usmani, R. Sloboda, and M. Tavakoli, "A Hand-Held Assistant for Semiautomated Percutaneous Needle Steering," *IEEE Trans. Biomed. Eng.*, vol. 64, no. 3, pp. 637–648, March 2017.

[11] S. E. Salcudean, T. D. Prananta, W. J. Morris, and I. Spadinger, "A robotic needle guide for prostate brachytherapy," in *Proc. IEEE Int. Conf. Robotics and Automation (ICRA)*, May 2008, pp. 2975–2981.

[12] C. M. Schneider, A. M. Okamura, and G. Fichtinger, "A robotic system for transrectal needle insertion into the prostate with integrated ultrasound," in *Proc. IEEE Int. Conf. Robotics and Automation (ICRA)*, vol. 1, May 2004, pp. 365–370.

[13] D. Y. Song, E. C. Burdette, J. Fiene, E. Armour, G. Kronreif, A. Deguet, Z. Zhang, I. Iordachita, G. Fichtinger, and P. Kazanzides, "Robotic needle guide for prostate brachytherapy: Clinical testing of feasibility and performance," *Brachytherapy*, vol. 10, no. 1, pp. 57–63, Jan. 2011.

[14] S. Basu, J. Tsai, and A. Majewicz, "Evaluation of tactile guidance cue mappings for emergency percutaneous needle insertion," in *2016 IEEE Haptics Symposium (HAPTICS)*, April 2016, pp. 106–112.

[15] G. Fichtinger, A. Deguet, K. Masamune, E. Balogh, G. S. Fischer, H. Mathieu, R. H. Taylor, S. J. Zinreich, and L. M. Fayad, "Image overlay guidance for needle insertion in CT scanner," *IEEE Trans. Biomed. Eng.*, vol. 52, no. 8, pp. 1415–1424, July 2005.

[16] G. S. Fischer, A. Deguet, C. Csoma, R. H. Taylor, L. Fayad, J. A. Carrino, S. J. Zinreich, and G. Fichtinger, "MRI image overlay: Application to arthrography needle insertion," *Computer Aided Surgery*, vol. 12, no. 1, pp. 2–14, Jan. 2007.

[17] O. Gerovich, P. Marayong, and A. M. Okamura, "The effect of visual and haptic feedback on computer-assisted needle insertion," *Computer Aided Surgery*, vol. 9, no. 6, pp. 243–249, April 2004.

[18] D. Magee, Y. Zhu, R. Ratnalingam, P. Gardner, and D. Kessel, "An augmented reality simulator for ultrasound guided needle placement training," *Med. Biol. Eng. Comput.*, vol. 45, no. 10, pp. 957–967, July 2007.

[19] C. Rossa, J. Fong, N. Usmani, R. Sloboda, and M. Tavakoli, "Multiactuator Haptic Feedback on the Wrist for Needle Steering Guidance in Brachytherapy," *IEEE Robot. Autom. Lett.*, vol. 1, no. 2, pp. 852–859, Feb. 2016.

[20] N. Abolhassani, R. Patel, and F. Ayazi, "Minimization of needle deflection in robot-assisted percutaneous therapy," *Int. J. Med. Robot.*, vol. 3, no. 2, pp. 140–148, June 2007.

[21] R. J. Webster, J. S. Kim, N. J. Cowan, G. S. Chirikjian, and A. M. Okamura, "Nonholonomic modeling of needle steering," *Int. J. Rob. Res.*, vol. 25, no. 5-6, pp. 509–525, May 2006.

[22] K. Reed, A. Majewicz, V. Kallem, R. Alterovitz, K. Goldberg, N. Cowan, and A. Okamura, "Robot-assisted needle steering," *IEEE Robotics Automation Magazine*, vol. 18, no. 4, pp. 35–46, Dec. 2011.

[23] B. Fallahi, M. Khadem, C. Rossa, R. Sloboda, N. Usmani, and M. Tavakoli, "Extended Bicycle Model for Needle Steering in Soft Tissue," in *Proc. IEEE/RSJ Int. Conf. Intelligent Robots and Systems (IROS)*, Oct. 2015, pp. 4375–4380.

[24] J. Carriere, C. Rossa, R. Sloboda, N. Usmani, and M. Tavakoli, "Real-time needle shape prediction in soft-tissue based on image segmentation and particle filtering," in *Proc. IEEE Int. Conf. Advanced Intelligent Mechatronics (AIM)*, July 2016, pp. 1204–1209.

[25] J. M. Gere and S. P. Timoshenko, *Mechanics of Materials*. Boston, MA: Springer US, 1991.